



HAL
open science

Late-Holocene palaeoenvironmental reconstruction from a lake in the Amazon Rainforest-Tropical Savanna (Cerrado) boundary in Brazil using a multi-proxy approach

Kury Milena Souza, Moreira Luciane Silva, Cordeiro Renato Campello, Abdel Sifeddine, Turcq Bruno, Stríkis Nicolás Misailidis, Santos Matheus Simões

► To cite this version:

Kury Milena Souza, Moreira Luciane Silva, Cordeiro Renato Campello, Abdel Sifeddine, Turcq Bruno, et al.. Late-Holocene palaeoenvironmental reconstruction from a lake in the Amazon Rainforest-Tropical Savanna (Cerrado) boundary in Brazil using a multi-proxy approach. *The Holocene*, 2021, 10.1177/09596836211019091 . ird-03688670

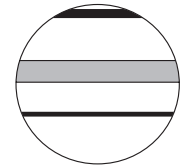
HAL Id: ird-03688670

<https://ird.hal.science/ird-03688670v1>

Submitted on 5 Jun 2022

HAL is a multi-disciplinary open access archive for the deposit and dissemination of scientific research documents, whether they are published or not. The documents may come from teaching and research institutions in France or abroad, or from public or private research centers.

L'archive ouverte pluridisciplinaire **HAL**, est destinée au dépôt et à la diffusion de documents scientifiques de niveau recherche, publiés ou non, émanant des établissements d'enseignement et de recherche français ou étrangers, des laboratoires publics ou privés.



Late-Holocene palaeoenvironmental reconstruction from a lake in the Amazon Rainforest-Tropical Savanna (Cerrado) boundary in Brazil using a multi-proxy approach

Kury Milena Souza,^{1,2}  Moreira Luciane Silva,¹ Cordeiro Renato Campello,¹ Sifeddine Abdelfettah,^{3,4} Turcq Bruno,³ Strikis Nicolás Misailidis¹ and Santos Matheus Simões¹

The Holocene
1–13
© The Author(s) 2021
Article reuse guidelines:
sagepub.com/journals-permissions
DOI: 10.1177/09596836211019091
journals.sagepub.com/home/hol


Abstract

As an ecotone, the region between the Amazon Rainforest and Tropical Savanna (Cerrado) biomes is, by definition, more susceptible to climate change. Therefore, understanding palaeoenvironmental dynamics is essential to address the future responses of such transition areas to climatic fluctuations. In this context, we present a new sediment record for the Late-Holocene retrieved from Barro-Preto, currently an oxbow lake located in an ecotone at the southern Brazilian Amazon border. Our multi-proxy data include carbon and nitrogen isotopes, as well as bulk TOC, chlorophyll derivatives, grain-size and microcharcoal analyses, all anchored on a radiocarbon-dated chronology. The sedimentary process recorded at the Barro-Preto Lake responded to both local and regional climate dynamics. It was influenced by river excursions associated to local responses to precipitation changes by the activation of the palaeochannel connecting the main-stem river and the Barro-Preto lake. This activation was evidenced by the presence of different colour lithology laminations accompanied by coarser sediments and also by climate conditions known to influence the Amazon region. Depositional processes linked to lake dynamics and different oxbow lake cycle stages were also important to explain the changes verified in the Barro-Preto record, endorsing the use of this lake formation for palaeoclimatic reconstructions. The record indicated a rising humidity trend, reflected by a progressive increase in lacustrine productivity, in accordance to other studies carried out in the Amazon region concerning the Late-Holocene, associated with a more southward displacement of the Intertropical Convergence Zone. Despite this rising humidity trend, dry episodic events during the Late-Holocene were evidenced by charcoal data, also coherent with regional Amazon studies, albeit exhibiting increased intensity, suggesting that the transitional nature of the environment might have influenced susceptibility to fires.

Keywords

Amazon basin, charcoal, ecotone, organic matter, oxbow lake dynamics, palaeolimnology

Received 29 July 2020; revised manuscript accepted 6 April 2021

Introduction

The Amazon plays a vital role in the global climate system, influencing precipitation (Cheng et al., 2013) and carbon cycles in both hemispheres (Olivares et al., 2015). With rising concerns on how global climatic changes will affect the environment, it is paramount to understand climate-environment interaction mechanisms, especially in such a region as the Amazon. In this context, reconstructions regarding environmental responses to past climate alterations may assist in predicting the magnitude and timing of future natural feedback to these changes.

Palaeoclimatic studies show that a dryer phase occurred in several areas in the Amazon basin during the Mid-Holocene (MH, ca. 6 ka) (Absy et al., 1991; Bush et al., 2007; Cordeiro et al., 2008; Moreira et al., 2013a; Pessenda et al., 2001; Sifeddine et al., 1994; Vidotto et al., 2007). This dryness may have been caused by a weakened South American Monsoon System (SAMS) and an associated northwards displacement of the Intertropical

Convergence Zone (ITCZ) (Cruz et al., 2005; Wolff et al., 2010). A return to more humid conditions then ensued in the Late-Holocene (LH) (Aniceto et al., 2014; Burbridge et al., 2004; Cordeiro et al., 2008; Mayle et al., 2000).

¹Departamento de Geoquímica, Universidade Federal Fluminense, Niterói, Rio de Janeiro, Brazil

²Fundação Cearense de Meteorologia e Recursos Hídricos (FUNCEME), Fortaleza, Ceará, Brazil

³LOCEAN Laboratory, IRD-Sorbonne Universités (UPMC, Univ Paris 06)-CNRS-MNHN, Bondy, France

⁴ERC2-Université de Quisqueya. Port au Prince - Haïti

Corresponding author:

Kury, Milena Souza, Fundação Cearense de Meteorologia e Recursos Hídricos (FUNCEME), Av. Rui Barbosa, 1246 – Aldeota, Fortaleza – CE, Fortaleza, Ceará 60115-221, Brazil.
Email: milenaskury@gmail.com

The extension to which vegetation distribution is altered in response to different climatic fluctuations in the Amazon is highly debated (Bush and de Oliveira, 2006; De Toledo and Bush, 2008; Nolan et al., 2018; Van Der Hammen and Hooghiemstra, 2000). While some studies suggest that no forest replacement by savannas associated with climate shifts during the Holocene took place (Bush et al., 2004; Castro et al., 2013; Colinvaux et al., 1996), fluctuations in boundaries from savanna to forest biomes during the Holocene have been observed for several Amazon regions (Desjardins, 1996; Pessenda et al., 1998a, 1998b, 2001). A recent modelling effort indicated that global temperature changes due to greenhouse gas emissions could lead to significant compositional and structural changes in the vegetation of the Neotropics by the end of the 21st century (Nolan et al., 2018).

Forest-savanna ecotones can respond to climatic fluctuations by altering their extensions according to edaphic conditions and moisture availability, associated to changes in precipitation distributions throughout the year (seasonality) (Behling and Hooghiemstra, 2000a; Silverio et al., 2013; Staver et al., 2011). Ecotones are, therefore, more susceptible to landscape modifications (Alencar et al., 2006). The present distribution of these boundary ecosystems in the Amazon region seems to be related to past climate fluctuations (Desjardin, 1996).

Oxbow lakes are residual water bodies resulting from the lateral migration of river channels across floodplains (Esteves, 1998). Common to practically all floodplains, oxbow lakes are an important source for palaeoenvironment reconstitutions. In general, the depositional sequence of an oxbow lake comprises coarse sediments deposited during the fluvial phase at the bottom, followed by a fining upward sequence, composed by mud as the system evolves to a lacustrine environment (Hudson et al., 2012; Wren et al., 2008). The oxbow-lake formation can be briefly categorized into four phases: an active meander bend (phase I), the detachment of the lake by a neck cut-off (phase II), the full lacustrine environment (phase III) and, lastly, the terrestrial phase (phase IV) (Wren et al., 2014). Monitoring studies exploring the hydrologic connectivity between oxbow lakes and main-stem rivers during flood events indicate that the influence of floodplains can, however, persist even in matured-phased oxbow lakes, such as those in lacustrine phase III (Hudson et al., 2012).

The hydrologic connectivity observed in a mature-phased oxbow lake, however, involves complex surface pathways associated with notched channels and floodplain swales (Hudson et al., 2012). In this scenario, flood events play an important depositional history role throughout episodic allogenic inputs well recognized in the sedimentary sequence by peaks in coarse sediments, high depositional rates and decreased organic material content. Our results provide important insights to past environmental conditions in a transitional area in the Amazon by exploring the relationship between local sedimentary and organic proxies and their interpretations and comparing them with several paleoclimatic archives from the Amazon basin.

The aims of this study were, therefore, to (1) detect whether bulk geochemical analyses of a lake situated in an ecotonal area could contribute to the understanding of Forest-Savanna dynamics; (2) understand past hydrological changes in said lake; and (3) characterize the past environment-climate links of the lake. To this end, we used a depositional sequence from an oxbow lake located in the ecotonal zone between the Amazon Rainforest and Tropical Savanna (Cerrado) biomes to recover past local and regional environmental changes in southern Amazon.

Study site

Barro-Preto is an oxbow lake formed by an abandoned meander of the Teles Pires River, a major Tapajós River tributary, and is located in Sinop, a city in northern Mato Grosso (Figure 1). The

elevation difference is ca. 4 m between the Teles Pires River (305 m) and the sampling point (309 m), although a higher vegetation patch at ca. 313 m exists between them, which would need to be surpassed in order for water from the main river to reach Barro Preto lake. The elevation profile is based on Google Earth Pro estimations.

Land use in the state of Mato Grosso began in the 1970s, with government incentives to make the Amazon region fit their new economic aspirations, especially after the construction of the roadway BR-163 in 1976 connecting Mato Grosso's capital of Cuiabá to Santarém, in the state of Pará (Araújo, 2008). Thereafter, Mato Grosso became a massive soybean producer, responsible for one third of Brazil's grain production (Richards, 2018), at the expense of forested areas. From 1988 to 2018, a total of 14.5 million ha of Amazon forests were cleared from the state. Mato Grosso also experienced a pasture area expansion from 2001 to 2017 (Simoes et al., 2020). The land-use change at the Sinop municipality is in accordance with the state's trend, where a large portion of the city comprises soybean farming areas and pastures, while the urban area is not as expressive (Simoes et al., 2020).

The local climate is tropical with a dry winter season (Aw) as classified by the Köppen-Geiger system, with precipitations occurring during December, January and February (austral summer), and a dry season in June, July and August (austral winter). The region presents a high annual mean precipitation, of about 1830 mm, and mean temperature of 25.2°C (based on data from Diamantino station, Instituto Nacional de Meteorologia (INMET), 2019). The vegetation comprises a transition from Cerrado vegetation to a broadleaf rainforest characteristic of the Amazon Equatorial Forest. The main local taxa include *leguminosae*, *annonaceae*, *lauraceae*, *euphorbiaceae*, *bursereae*, *cecropiaceae*, *melastomataceae*, *rubiaceae* and *sapindaceae* (Araújo, 2008).

Material and methods

Sampling and core description

The Barro-Preto Lake core (BP-1502) (3.84 m long) was sampled using a vibro-core system at the northern section of the lake (55° 41' 15" W; 11° 45' 28" S; Figure 1), at a depth of approximately 2 m. The core was opened at the UFF Sedimentology Laboratory and its texture and colour patterns were described according to the Munsell system (Munsell, 2000), as presented in Table 1. A sub-sampling was carried out in one half of the core using a u-channel at each centimetre, to calculate dry bulk density. To this end, the samples were dried until constant weight in a muffle-furnace and their final weight noted. Subsequently, this dry weight was divided by the sample volume (1.5 cm³) to obtain the dry bulk density, in g.cm³. The same half was then sliced at 1 cm intervals. The other half was packed and frozen for further analyses.

Radiocarbon dating

The chronology of the BP-1502 core was based on eight ¹⁴C measurements of the bulk organic matter (Table 1). The analysis was carried out at two laboratories, the Laboratoire de Mesure du Carbone 14, (LMC14-France) and the International Chemical Analysis Inc. (Miami, USA). The obtained ages were calibrated by the CLAM software (Blaauw, 2010) using the SHCal20.14C calibration curve (Hogg et al., 2020; Table 1). The chronological model was also determined by the CLAM software, using a smooth-spline model with smoothness=0.5 to reduce sediment package artefacts (Figure 2).

Grain size analysis

Grain size was determined by a laser granulometer model CILAS 1064 at the UFF Sedimentology Laboratory. The samples

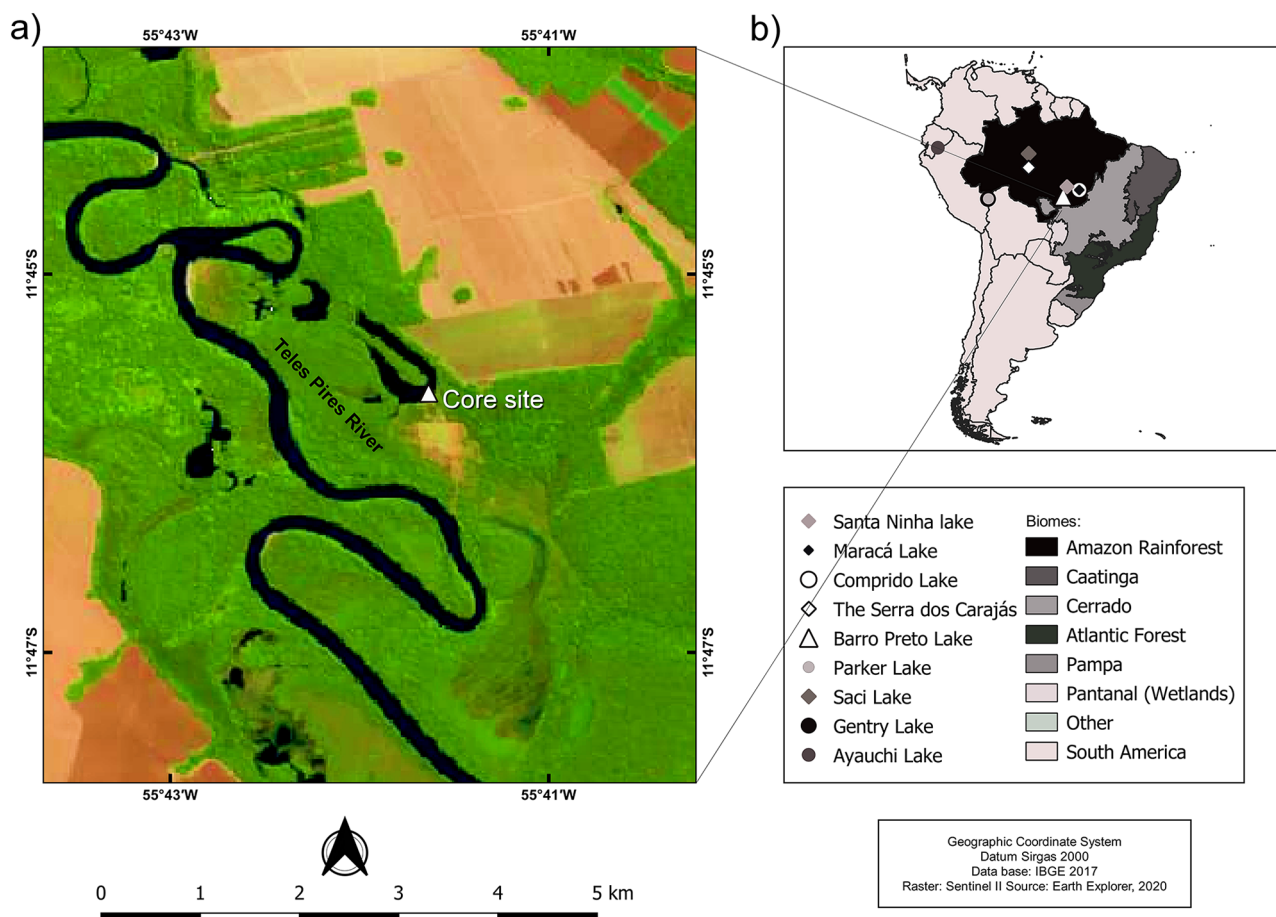


Figure 1. Study area. Brazilian biome distribution in grayscale (b), with the triangle indicating the location of Barro-Preto lake, with a satellite image of the oxbow lake and the Teles Pires river (a). Main paleoclimatic records used in the discussion of this paper are also shown in the map (b).

Table 1. Radiocarbon dating and calibration of core BP-1502 samples.

Laboratory code	Depth (cm)	$\delta^{13}\text{C}$ (‰)	^{14}C date (yr BP)	Calibrated age (cal yr BP)	Significance interval (95%)
ICA-17OS/1069	9–10	−32.0	50 ± 30	171	95–229
SacA49819	19–20	−33.3	520 ± 30	342	235–405
SacA49820	56–57	−34.0	750 ± 30	779	696–880
ICA-17OS/1070	69–70	−32.0	990 ± 30	898	819–989
SacA60923	113–114	−33.5	1275 ± 30	1216	1150–1295
ICA-18OS/0401	149–150	−29.6	1660 ± 30	1414	1337–1490
SacA49821	229–230	−32.8	1735 ± 30	1644	1582–1726
ICA-18OS/0402	299–300	−28.3	2120 ± 30	2089	2042–2185
ICA-17OS/1071	359–360	^a	2730 ± 30	2771	2685–2823

^a $\delta^{13}\text{C}$ value not available.

underwent a pre-treatment during 8 months with weekly 5 mL H_2O_2 applications to remove organic matter (the time of H_2O_2 application varied per sample, as some samples stopped reacting before others). The peroxide was removed by adding 30 mL of distilled water to the samples, followed by centrifugation for 5 min at 3500 rpm. The supernatants were discarded and the process was repeated until a transparent supernatant was obtained. Then, 40 mL of a dispersal agent (sodium hexametaphosphate, 4%) were added to the samples, which were then mixed using a shaker table for 24 h before being analysed by laser granulometry. Grain sizes were categorized as coarse silt (31–16 μm), medium silt (16–8 μm), fine silt (8–4 μm), very fine silt (4–2 μm) and clay (>2 μm) (Udden, 1914; Wentworth, 1922). As the clay and very fine silt fractions were significantly correlated, they were combined as “Clay + VFS.”

Isotopic and elemental analyses

Ninety-nine aliquots were ground, homogenized, dried until constant weight and wrapped in tin capsules of ca. 2 g. They were then sent to the Laboratoire de Mesure du Carbone 14, IRD-Bondy, wherein isotopic and elemental carbon and nitrogen were analysed by a PDZ Europa ANCA-GSL elemental analyser with an interface for a PDZ Europe 20–20 isotope ratio mass spectrometer. Carbon-13 and ^{15}N isotope values were expressed in δ units (‰), referring to the vPDB international standard and atmospheric dinitrogen values, respectively.

Chlorophyll derivative analysis

Chlorophyll derivatives from sixty-nine previously frozen aliquots were extracted using 90% acetone, and their absorbances

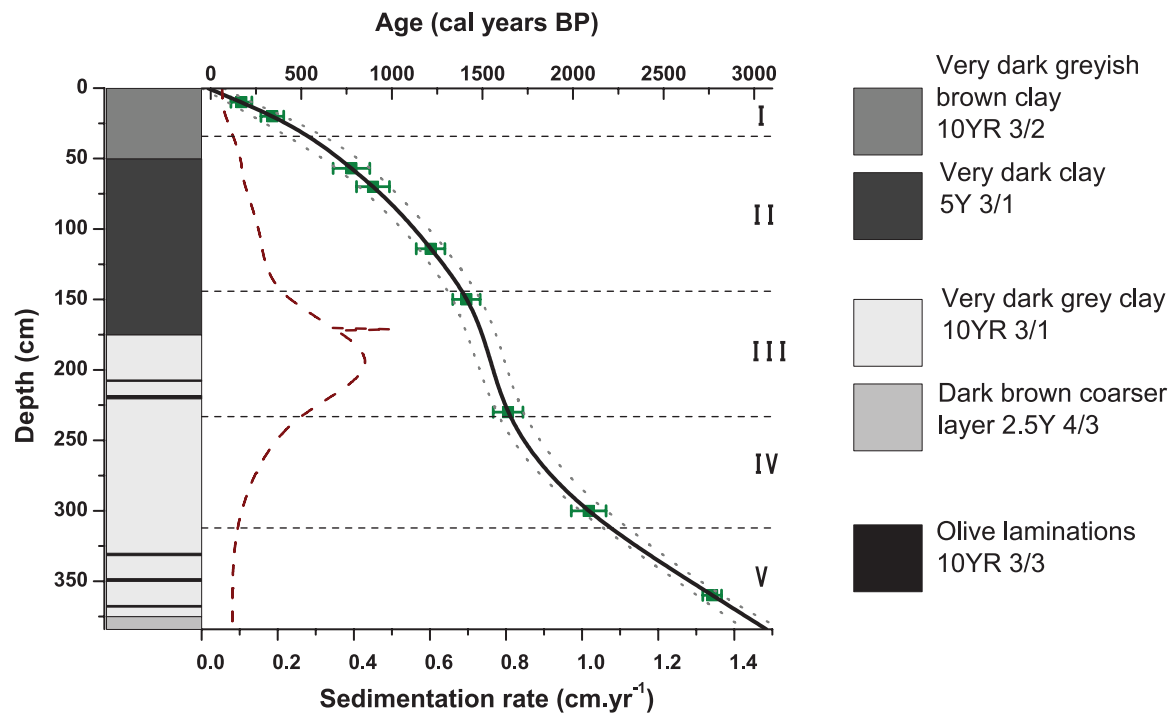


Figure 2. Core BP-1502 stratigraphy indicating the geochronology model and sedimentation rates. Colour codes are based on Munsell (2000). The solid black line represents the modelled data, and dotted lines, the error. Boxplot markers comprise the dated samples with the error range, while the dashed line is the estimated sedimentation rate. Units are represented by Roman numerals on the right side of the graph.

were determined using a scanning spectrophotometer at the 350–800 nm interval. Background correction was performed through baseline subtraction from 500 to 800 nm. Pigment concentrations are reported as Sedimentary Pigments Degradation Units (SPDU) (Valentyne, 1955), an arbitrary unit, where 1 SPDU represents an absorbance of 1.0 in a 10 cm cell using 100 mL of acetone as a solvent for 1.0 g of OM (Cordeiro et al., 2008).

Carbon accumulation rate analysis

First, the number of particles per gram of analysed sample was calculated by dividing the number of particles per slide by the mass of sample filtered for each slide (grams). Then, carbon accumulation rates (CAR) were calculated by multiplying the sample bulk density, number of particles per gram of analysed sample and sediment accumulation rates generated by the age-depth model and is expressed as $\text{particles.cm}^{-2}.\text{y}^{-1}$.

Microscopic charcoal analysis

The microcharcoal analysis was carried at the UFF Sedimentology and Optical Laboratories. Ninety-three humid sediment samples underwent humic acid removal with a 20% NaOH solution, followed by agitation, centrifugation and supernatant removal. This process was repeated until a transparent supernatant was obtained. The samples treated with this alkaline solution were washed with distilled water and stored in a 100 mL water solution. From this solution, 2 mL were agitated and then filtered through previously weighed Millipore acetate cellulose filters. The samples were then maintained in a furnace until dry and were then weighed. The dry filters were then dissolved in acrylic slides using Ethyl Acetate and the laminae were observed under an optic microscope at 250 \times magnification and the charcoal particles were counted ten times per slide. The particles were observed using the IMAQ Vision Builder software and the morphological charcoal characteristics were noted. Method adapted from Cordeiro et al. (2008).

Statistical analyses

A principal component analysis (PCA) using normalized data-series was also performed to separate common variables among the proxies throughout the analysed core. To this end, first we did a linear interpolation of the data at every 1 cm using the PAST 4.03 software (Hammer et al., 2001). Then, the records were normalized using the following equation:

$$nx = \frac{(x - \bar{x})}{\sigma}$$

Where nx is the normalized data, x is the original data and \bar{x} and σ are, respectively, the mean and the standard deviation values. After this process, the PCA was generated using Python 3 (Van Rossum and Drake, 2009). The aim of this analysis was to determine proxy covariations, in order to understand which processes were most important within the lake at different depths.

Results

Chronology and lithology

The BP-1502 chronological model is based on eight TOC AMS radiocarbon dates, presenting a calibrated basal age of ca. 3070 calendar years before the present (cal yr BP; Table 1 and Figure 2). Geochemical result integration allowed for the identification of five sedimentary Units in the BP-1502 core record, namely Unit-V (384–312 cm; ca. 3067–2209 cal yr BP), Unit-IV (312–233 cm; ca. 2209 to 1655 cal yr BP), Unit-III (233–144 cm; ca. 1655–1387 cal yr BP), Unit-II (144–34 cm; ca. 1387–537 cal yr BP) and Unit-I (34–0 cm; ca. 537 cal yr BP to present). Unit-V shows a low average sedimentation rate of ca. 0.084 cm.yr^{-1} , while higher values were observed in Units IV and III, with average values of 0.155 cm.yr^{-1} and 0.347 cm.yr^{-1} , the latter comprising the highest average of all units. Sedimentation rates decreased expressively in Units II and I, with average values of 0.137 cm.yr^{-1} and 0.063 cm.yr^{-1} , respectively.

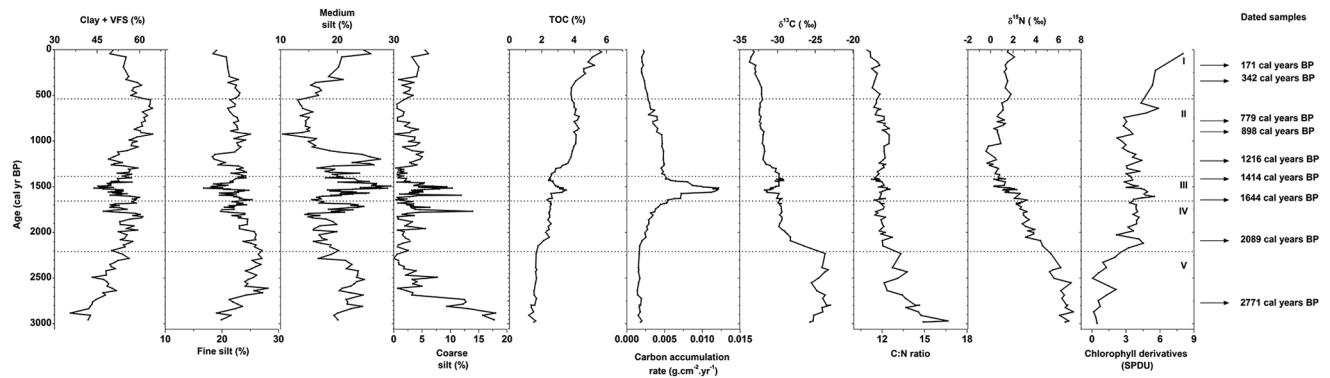


Figure 3. Grain-size percentage variations, bulk and isotope proxies along the BP-1502 core chronology. Roman numerals in the left indicate the Units, while dated points and their respective age are shown in the far right.

The lithological description presented in Figure 2 indicates that Unit-V is composed of a marked dark brown horizon in the bottom, while Units V and IV present very dark grey silty clay sediments. Unit-III and Unit-II present mostly very dark clay sediments whereas Unit-I is characterized by very dark greyish brown sediments. Olive laminations were observed in Unit-V at 367.5 cm and ca. 1.20 cm thick, 348 cm with ca. 2 cm, 330 cm with ca. 1.80 cm and in Unit-III at 220 cm, with ca. 2.40 cm and at 207 cm, with ca. 1 cm (Figure 2).

Grain size analyses

The sediment grain size analyses of the BP-1502 core indicated the predominance of very fine-grained sediments ($<4\mu\text{m}$) with increased contribution of coarse silt in Units V and III (Figure 3). Unit-V is characterized by the highest coarse silt values recorded in the core, with an average of 6.04%, and the second highest medium silt value, averaging 21.9%, while average clay + very fine silt and fine silt values were 47.3 and 24.4%, respectively. A decrease in grain-size in Unit-IV is noted, with an average clay + very fine silt content of 54.8% and fine silt percentage of 23.5%, while the average coarse and medium silt percentages were 2.90% and 18.8%, respectively. Unit-III indicates an increase in the average coarse and medium silt percentages of 4.05% and 22.4%, respectively. In contrast, fine silt and very fine silt + clay reduced to average percentages of 21.4% and 52.1%, respectively. Unit-II exhibits decreased grain size, attested by higher clay + very fine silt and fine silt percentages and lower medium and coarse silt values, averaging values of 57.7%, 22.3%, 17.6% and 2.40%, respectively. Unit-I displays a small increase in coarse and medium silt contents, with average values of 3.23% and 18.8%, respectively whereas clay + very fine silt values decreased to 56.3% and fine silt, decreased to 21.6%

Organic proxy analysis

Unit-V is characterized by the lowest TOC values, averaging 1.56 wt.% (Figure 3). A progressive increase in the organic content is observed in Unit-IV, which presented an average TOC value of 2.44 wt.%. This increase continued until Unit-III, reaching an average of 2.87 wt.% increasing up to Unit-I. The highest TOC values were observed in Units II and I, with average values of 3.81 wt.% and 4.81 wt.%, respectively. The lowest TOC values that characterized the Unit-V were accompanied by the highest C:N atomic ratio, averaging 13.7 (Figure 3). A decrease in this ratio can be observed in Unit-IV, with an average of 11.9. No expressive changes were detected in the C:N ratio of Units III, II and I, which contained average values of 12.0, 12.0 and 11.4 respectively.

Unit-V presents the most enriched carbon isotopic values, at -24.4‰ (Figure 3). A decrease in $\delta^{13}\text{C}$ values is observed in

Unit-IV, which presented an average of -29.4‰ . A slight decrease in these values was noted in Unit-III, with average values of -30.3‰ . Isotopic values decrease further in Units II and I, averaging -31.8‰ and -33.0‰ , respectively. The nitrogen isotopic composition of the lowermost core section is characterized by the highest $\delta^{15}\text{N}$ values, with an average of 6.21‰ (Figure 3). A decrease in these values is observed in Units IV, III and II, with average values of 3.10‰, 1.29‰ and 0.80‰, respectively. In contrast, an increase in $\delta^{15}\text{N}$ was noted in Unit-I, with an average value of 1.49‰.

Sedimentary pigments and CAR were lowest in Unit-V, with averages of 1.00 SPDU and $16.7\text{ g.m}^{-2}\text{.y}^{-1}$, respectively (Figure 3). An increase in the concentration of sedimentary pigments was observed in Units IV and III, with average values of 3.70 and 4.10 SPDU, respectively. CAR values increased in Unit-IV, averaging $35.1\text{ g.m}^{-2}\text{.y}^{-1}$, reaching a peak in Unit-III, with an average value of $86.7\text{ g.m}^{-2}\text{.y}^{-1}$. A decrease in these values was detected in Unit-II, with an average sedimentary pigment value of 3.47 SPDU and CAR value of $40.7\text{ g.m}^{-2}\text{.y}^{-1}$. Unit-I is characterized by the highest chlorophyll derivative concentrations recorded in the BP-1502 core, averaging values 6.31 SPDU. While an increase in sedimentary pigments is observed, CAR values decreased to $21.3\text{ g.m}^{-2}\text{.y}^{-1}$, probably due to the low sedimentation rate of this unit.

Microscopic charcoal examination

Microcharcoal particles were found in all 92 samples observed, with a minimum count of 32 particles at the sample from depth 96 cm. Average particles count through the core was ca. 122 and maximum value was 226 at depth 364 cm.

Unit-V charcoal particles size ranged from 19.2 to $70.4\mu\text{m}$, averaging average of $33.1\mu\text{m}$. Charcoal accumulation rates contained a maximum of $7.27 \times 10^5\text{ particles cm}^{-2}\text{ y}^{-1}$, averaging $4.07 \times 10^5\text{ particles cm}^{-2}\text{ y}^{-1}$, with a minimum of $1.77 \times 10^5\text{ particles cm}^{-2}\text{ y}^{-1}$. Concerning Unit-IV, charcoal sizes ranged from 11.5 to $42.6\mu\text{m}$, with average value of $24.5\mu\text{m}$, while charcoal accumulation rates varied from $1.19 \times 10^6\text{ particles cm}^{-2}\text{ y}^{-1}$ to $2.78 \times 10^5\text{ particles cm}^{-2}\text{ y}^{-1}$, with an average of $7.00 \times 10^5\text{ particles cm}^{-2}\text{ y}^{-1}$. Unit-III contained minimum charcoal size of 18.9 μm , maximum of $73.4\mu\text{m}$ and average of $29.0\mu\text{m}$. Charcoal accumulation rates in this unit ranged between a peak of $2.69 \times 10^6\text{ particles cm}^{-2}\text{ y}^{-1}$ and $6.76 \times 10^5\text{ particles cm}^{-2}\text{ y}^{-1}$, averaging $1.66 \times 10^6\text{ particles cm}^{-2}\text{ y}^{-1}$. Units II and I were characterized by the lowest charcoal size values, with minimum values of 1.32 and $12.5\mu\text{m}$, maximum of 48.8 and $69.2\mu\text{m}$ and average values of 22.7 and $22.6\mu\text{m}$, respectively. Charcoal accumulation rates for Unit-II comprised a maximum of $1.67 \times 10^6\text{ particles cm}^{-2}\text{ y}^{-1}$, minimum of $2.16 \times 10^5\text{ particles cm}^{-2}\text{ y}^{-1}$ and average of $8.33 \times 10^5\text{ particles cm}^{-2}\text{ y}^{-1}$, whereas charcoal accumulation

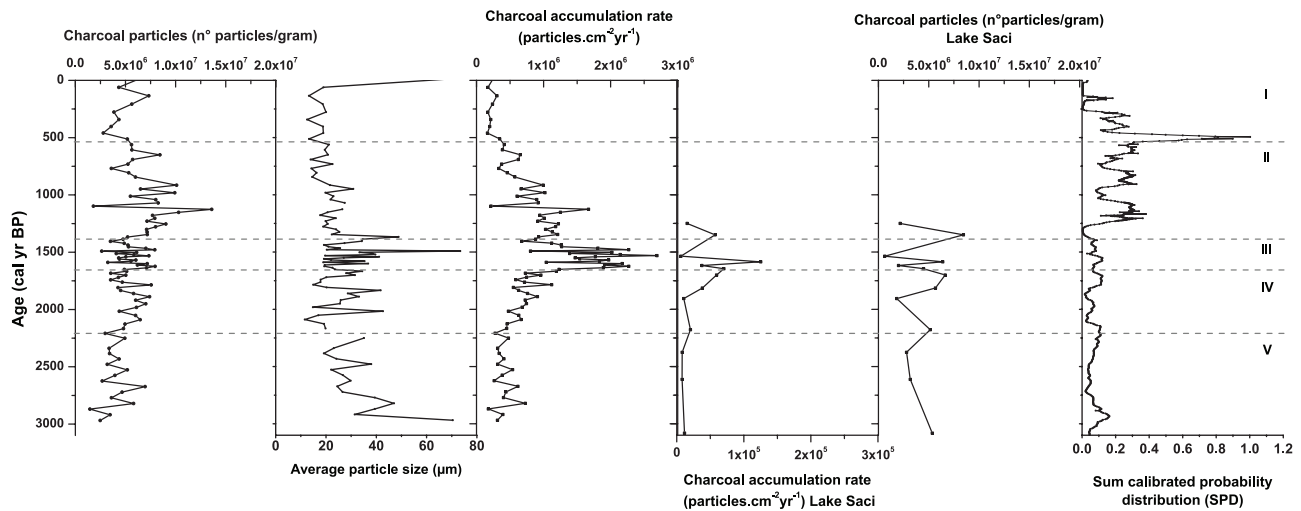


Figure 4. Comparison between charcoal data from Barro-Preto Lake (concentration, size and charcoal accumulation rate) and charcoal data from Sac Lakei, South Amazon (Fontes et al., 2017), and archaeological site distribution in the Eastern Amazon (Maezumi et al., 2018). High values of Sum calibrated probability distribution indicate increased human influence.

rates in Unit-I decreased, ranging from 3.45×10^5 particles $\text{cm}^{-2} \text{y}^{-1}$ to 1.64×10^5 particles $\text{cm}^{-2} \text{y}^{-1}$, averaging 2.28×10^5 particles $\text{cm}^{-2} \text{y}^{-1}$ (Figure 4).

Unit-V presented concentration values of particles per gram ranging from 6.95×10^6 to 1.45×10^6 particles/g, with an average of 3.96×10^6 particles/g. In Unit-IV, values reached a maximum of 7.56×10^6 , a minimum of 2.97×10^6 and an average of 5.22×10^6 particles/g. Unit-III maintained similar values, ranging from 7.95×10^6 to 2.63×10^6 , averaging of 5.53×10^6 particles/g. The number of charcoal particles per gram peaked in Unit-II at 1126 and 1152 cal yr BP, with values of 1.36×10^7 (maximum value at this Unit) and 1.03×10^7 particles/g. IN this Unit, minimum and average values were, respectively, of 1.80×10^6 and 7.06×10^6 particles/g. The topmost Unit presented a maximum value of 7.32×10^6 , a minimum of 2.79×10^6 and average of 4.82×10^6 particles/g (Figure 4).

Discussion

Principal component analysis

The first two principal components explain ca. 71% of the total data variance. Principal component 1 (hereafter, PC1) displays a higher variation of organic proxies C:N, $\delta^{13}\text{C}$, $\delta^{15}\text{N}$, TOC, chlorophyll derivatives and also in charcoal concentration. The most altered grain fraction in this PC was clay + VFS, a granulometry usually associated with organic matter. This component probably represents the OM origin and variation within the core. Concerning principal component 2 (hereafter, PC2) grain-size data varied consistently, and, to a lesser degree, sedimentation-dependent proxies. Organic proxies were not significantly altered in this component. Chlorophyll derivatives were the most altered, mostly associated to increased grain-size, which may be linked to increased productivity during nutrient input episodes into the lake from eroded sediments. PC2 mostly represents changes in lake hydrodynamics.

Palaeoenvironment interpretations

Unit-V (384–312 cm; 3067–2209 cal yr BP). Unit-V lithology displaying laminations and low sedimentation rates is in tandem with the coarser granulometry (Figures 2 and 3), indicating that the lake still suffered the influence of the Teles Pires river during this Unit, with a more lotic environment hindering finer grain deposition. Unit-V would correspond to stage one of the oxbow

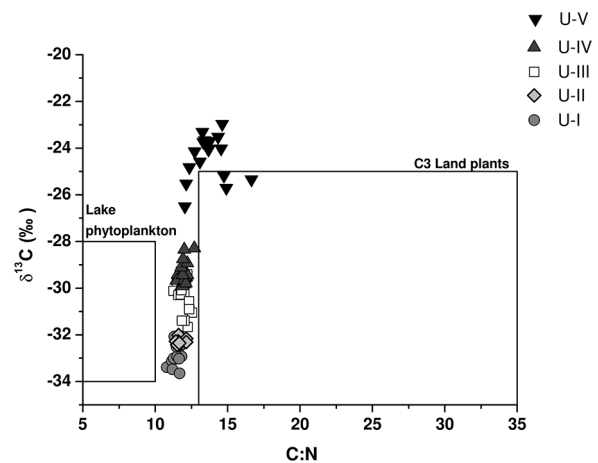


Figure 5. Cross diagram (C:N atomic ratio vs $\delta^{13}\text{C}$) for core BP-1502. Boundaries of major OM sources are adapted from Kim et al. (2012) and Moreira et al. (2013b).

lake cycle, an active meander bend (Wren et al., 2014) or at least to stage three, a lacustrine environment, with the influence of a flood pulse. In the PCA (Figure 6), Unit-V is associated mainly with PC2, which corroborates the interpretation of high hydrodynamics and grain-size variations, but also, to a lesser degree, with PC1, indicating variations in the origin of the OM and its processes within the lake, probably associated to the relationship between OM input and local productivity at an oxbow lake with fluvial system connections. CHAR and charcoal concentrations don't seem to be important in this unit. The ^{13}C -enriched carbon isotopic values in Unit-V, corroborated by the C:N ratio (Figure 5), suggest that Barro-Preto lake received a large proportion of land-derived cellulose-rich OM during this period (Meyers, 2003) from the local catchment area by erosion during river input. The carbon isotopic signal for Unit-V indicates a slight influence of C4 plants (Figure 5), suggesting a relatively drier environment. Unit-V is also characterized by the lowest core TOC values, sedimentary pigments and CAR (Figure 3), suggesting low productivity. The high average value of $\delta^{15}\text{N}$ in this unit (Figure 3) can reflect biological drawdowns of a limited nutrient pool (Meyers and Lallier-Vergès, 1999), associated with reduced nutrient availability as a result of low-productivity levels during this drier period. Although high $\delta^{15}\text{N}$ values can also result from

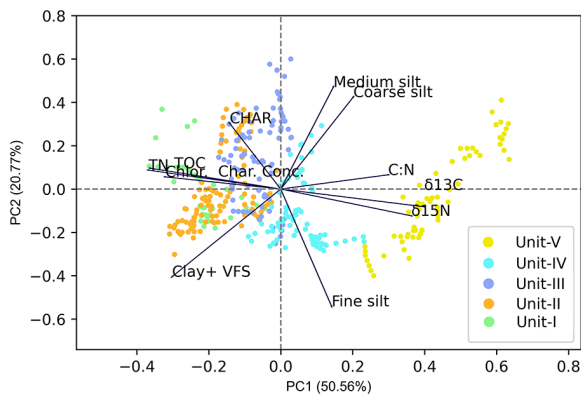


Figure 6. Principal component analysis indicating the analysed proxies coarse, medium and fine silt, clay +VFS, charcoal accumulation rate (CHAR), charcoal concentration, total organic carbon (TOC), total Nitrogen (TN), C:N ratio, chlorophyll derivatives (Chlor.), $\delta^{13}\text{C}$ and $\delta^{15}\text{N}$. Units are displayed in different colours (for coloured version of this image, please refer to the online version of this paper).

denitrification, Unit-V sediment data suggests a high-energy environment, thus allowing for well-oxygenated water and diminishing the probability of denitrification, that occurs in anoxic settings (Meyers and Teranes, 2001).

Average charcoal particle size is higher in this unit, particularly at the base of the core (Figure 4). Despite this, all charcoal particles found in BP-1502 core were $<125\ \mu\text{m}$, suggesting that the charcoal found in Barro-Preto lake does not necessarily originate from the lake watershed, but may, instead, provide an estimation of regional fires, as small particles can be windborne (Cordeiro et al., 2011). Charcoal concentrations in this unit are similar to those found in Saci lake (ca. 665 km to the north of Barro-Preto lake; Figure 4), strengthening the suggestion that charcoal fragments in Barro-Preto lake are representative of regional fire activity.

Unit-IV (312–233 cm; 2209–1655 cal yr BP). A transition to a more lentic circulation can be observed in Unit-IV, attested by a decrease in the coarse and medium silt fractions (Figure 3) and a more homogeneous lithology (Figure 2), suggesting river disconnection. Barro-Preto lake is disconnected from the main river, with contact only with the Teles Pires river during intense rain events, as discussed in the next section, through abandoned streams in the oxbow formation. Most of the variation observed in Unit-IV is associated to PC2, indicating the persistent importance of hydrodynamic processes in this Unit, mainly related to decreases in grain-size (Figure 6). As a consequence of the main channel cut-off, progressive increases in total organic carbon and sedimentary pigment contents were recorded in Barro-Preto lake sediments, indicative of high lacustrine productivity levels. In addition, the more depleted $\delta^{13}\text{C}$ values alongside a lower C:N ratio suggest a rising contribution of nitrogen-rich algae and phytoplankton to OM (Figure 5), linked to lake level and humidity increases. TOC are also increased, accompanied by increases in sedimentary pigments and CAR, corroborating the other organic and sedimentological proxies and indicating increased lake productivity (Figure 3). This productivity can be associated with higher lake-levels, coherent with the humid Late-Holocene. A decrease in average $\delta^{15}\text{N}$ values is indicative of lesser OM cycling through trophic levels, associated with greater nutrient availability (Meyers and Teranes, 2001).

Unit-III (233–144 cm; 1655–1387 cal yr BP). The lower hydrodynamic period of Unit-II was interrupted by a flooding event at

around 1630–1460 cal yr BP, characterizing Unit-III. This event comprises an increased sedimentation rate and a slightly coarser granulometry, as well as the presence of an olive lithology lamination (Figures 2 and 3, respectively), temporarily linking Barro-Preto lake to the Teles Pires river. The deposition of coarser sediments and the lack of ^{14}C -dates inversions suggest an influence of clastic material not from the river itself, which would be older than autochthonous OM, but from the neighbouring sand bank where the palaeochannel that connected the river to the lake was located, which was eroded during the flood pulse. This pulse indicates that Barro-Preto lake is in stage three of the oxbow lake cycle, a lacustrine state with possible connections to the river during flooding events (Hudson et al., 2012; Wren et al., 2014). The PCA correspondingly shows this Unit as highly influenced by PC2, indicating hydrodynamic processes as its main feature (Figure 6). Accordingly, the more variable proxies are coarser grain-sizes and sediment rate-dependent CHAR, strengthening the scenario of a higher energy system. The high sedimentation event matches an increase in TOC values as well as in sedimentary pigments and a decrease in $\delta^{13}\text{C}$ values. Indeed, the total organic carbon and carbon accumulation rate increases during this period (Figure 3), alongside increased pigments, may be a consequence of higher nutrient input during the flooding caused by river the connection. The decrease in $\delta^{13}\text{C}$ values suggests detritic C3 material being carried into the lake, which agrees with the erosion of the vegetation-covered sandbank, where a connecting channel is formed. As no expressive change in C:N ratios is observed, we assume that the material that entered the lake through the river connection, even if a result from palaeochannel erosion and, hence, higher in carbon content, was either present in small amounts and/or might have been balanced by the increasing lake productivity that would, in turn, increase OM nitrogen content. A further decrease in $\delta^{15}\text{N}$ rates may be due to higher allochthonous input, as this would both result in greater nutrient availability, which would then decrease nitrogen recycling, and carry typical terrestrial plant nitrogen levels to the lake (Fogel and Cifuentes, 1993; Meyers, 2003).

The increase in charcoal accumulation rates observed in this unit is also seen at Saci lake, although one order of magnitude lower. Maezumi et al. (2018) data does not indicate high human activity in the Amazon region during this period, suggesting climatic conditions as the main fire trigger detected in this unit. Indeed, seasonality variations, with a shorter period comprising intense rains and another presenting drought, could explain the higher fire activity and the flood event connecting Barro-Preto lake to the river. As a strong seasonality is characteristic of transitional zones (e.g. Behling and Hooghiemstra, 2000a; McMichael et al., 2012a), we could argue that such changes could occur in the ecotonal Barro-Preto lake setting.

Unit-II (144–34 cm; 1387 to 537 cal yr BP). The beginning of Unit-II indicates decreased TOC, potentially associated to the high sedimentation event detected in the previous Unit (Figure 3), suggesting a lithoclastic input contribution that could dilute sedimentary OM (Turcq et al., 2002). While the proportion of autochthonous and allochthonous OM verified by the C:N ratio did not vary significantly, the chlorophyll derivative signal decreases, indicating a slight drop in productivity as the increased amount of nutrients from the inundation events of Unit-III is used.

In Unit-II, the sedimentation rate returns to values similar to those prior to the river pulse in Unit-III, reducing in tandem with grain size, indicating lower hydrodynamics. This suggests that the Barro-Preto lake was again disconnected from the Teles Pires river during this Unit, still in the lacustrine phase three but without a flood pulse during this period. A slight decrease in $\delta^{13}\text{C}$ values is noted (Figure 3), demonstrating a clear trend towards a more humid environment beginning at 144 cm. Accordingly, TOC

values are increased along this unit, agreeing with the rising humidity and lake levels observed (e.g. Moreira et al., 2013a, 2013b; Moreira-Turcq et al., 2014), while CAR values decrease as sedimentation rates diminish. With an increasing OM supply, $\delta^{15}\text{N}$ continues low in Unit-II, representing low OM recycling rates in the water column. The PCA concerning this unit suggests the influence of fine-grained sediments, consistent with lower hydrodynamics. Variations in CHAR are also observed in this Unit's cluster in the PCA, suggesting important changes in this proxies during this unit, as discussed. In this context, the increased Clay + VFS contents are an important process during this phase, indicating the disconnection from the river influence and lake stabilization, coherent with the influence of PC2 in this Unit.

The microcharcoals, at their maximum in this Unit, represent a direct measure of forest fires, which can be linked to dry spells in rainforests, indicating regional consistency with data from across the Amazon (Cordeiro et al., 2014; Fontes et al., 2017; Hammond et al., 2006; McMichael et al., 2012a, 2012b; Rodríguez-Zorro et al., 2018; Santos et al., 2000). The fires of the Late-Holocene in Barro-Preto do not seem to have been enough to alter the surrounding lake environment, as no significant organic proxy changes were noted during peak microcharcoal concentrations. Despite this, charcoal accumulation rates in Barro-Preto lake are higher than those reported for Lake Saci and Carajás, suggesting that the transitional nature of Barro-Preto lake may have influenced vegetation susceptibility to forest fires. A human presence in the area may have also been the cause for forest ignition, as indicated by various archaeological and palaeoecological eastern Amazon occupation evidence throughout the Holocene (e.g. Maezumi et al., 2018, Figure 3; Bush et al., 2000) and taking into account that lakes were preferred settlement locations (McMichael et al., 2012a). Nevertheless, interpretations as to the extent that pre-Columbian populations altered the environment of this transitional lake are constrained by the applied methodology, as the bulk organic proxies indicate no evidence of large-scale environmental disturbances at Barro-Preto lake.

Unit-I (34–0 cm; 537 cal yr BP to present). Unit-I hydrodynamics indicates a slight increase in grain size, which may be attributed to a small marginal erosion during increasing lake levels under the more humid conditions of the Late-Holocene. The lower sedimentation rate in this Unit suggests lower sediment input, as the lake is disconnected from the river. Despite the input of coarse silt into the lake, possibly by marginal erosion, this grain-size corresponds to only 3.28% of the sediment in this unit, thus not a very significant factor concerning the general sedimentation rate trend, comprising mainly clay and very fine silt. Unit-I appears in the PCA as dependent mainly on PC2, indicating that lake hydrodynamic processes are also important in this unit. Chlorophyll derivatives, TOC and proxies dependent upon sedimentation are highlighted in this unit, indicating a lake with expressive productivity and OM availability, but also undergoing alterations in sedimentation processes (Figure 6).

Unit-I presents a decrease in average $\delta^{13}\text{C}$ values, indicating an increasing influence of C3 plants, typical of forests (–25.0‰ to –35.0‰, Moreira et al., 2013b) and phytoplankton (between –28.0‰ and –34.0‰, Araújo-Lima et al., 1986). The C:N ratio did not indicate any significant change, corresponding to a mixed OM origin, and is mainly autochthonous (Figures 3 and 5). TOC and sedimentary pigment values reached the highest values of the core in this unit, while CAR decreased due to slower sedimentation rates (Figure 3). These organic proxies suggest increasing productivity and higher lake levels, in accordance to the increasing humidity trend for the Late-Holocene in transitional Amazon areas (Behling and Hooghiemstra, 2000a; 2000b; Berrio et al.,

2000; Meneses et al., 2013; Pessenda et al., 1998a, 1998b). A higher average $\delta^{15}\text{N}$ value in this Unit seems to indicate a contribution of autochthonous organisms processes to the lake sediments, which would increase $\delta^{15}\text{N}$ (typical values for algae range between 7‰ and 10‰; Meyers, 2003).

Charcoal concentrations (particles/g) began to drop at around 460 cal yr BP, roughly synchronous with the European arrival in Brazil and matching other studies (e.g. McMichael et al., 2012a; Nevle and Bird, 2008). The last increase in the charcoal particle values was observed from 207 cal yr BP, accompanied by an increase in average charcoal size, which may indicate more relatively local burnings. This increase in fires at the top of BP-1502 core may be associated to a greater plant biomass availability and eventual dry events linked to the marked seasonality of the region.

Regional palaeoclimatic links

Mayle et al. (2000) reported evidence of a drier climate in the southern Amazon border prior to 2790 cal yr BP, through a palynology analysis of a Laguna Bella Vista sediment core. Lake levels were lower, and the savanna landscape was seasonally inundated. The period investigated in that study agrees in part with Unit-V, strengthening the interpretation of a relatively drier climate in this Unit. The Mid-Holocene, which is believed to have been mainly a dry phase in the Amazon (Absy et al., 1991; Bush et al., 2007; Cordeiro et al., 1997; Moreira et al., 2013a, 2013b; Sifeddine et al., 1994; Vidotto et al., 2007), was not recorded by the period of the BP-1502 core, although a clear transition to more humid climates can be seen from 3067 cal yr BP.

The bulk organic analysis of two Amazon lakes, Lakes N3 Carajás Serra Norte (Cordeiro et al., 2008) and Caracaranã, indicate an increase in lake productivity evidenced by a decrease in C:N values from 2000 cal yr BP to the present, with values ranging between 10 and 15 (Turcq et al., 2002), similar to the C:N range observed for Barro-Preto lake. Moreira et al. (2013a) also report rising productivity in two cores from Comprido lake, a north Amazon lake, from 3000 cal yr BP, with chlorophyll derivatives values between 4.1 and 7.1 SPDU and C:N ratios of 12 and 7. Carbon isotopic values at Comprido lake are also similar to the ones noted for Barro-Preto, with an average of –27.1‰ between 2600 and 1300 cal yr BP for one of the cores and –28.4‰ between 3000 and 300 cal yr BP for the other core.

Pollen evidence from eastern Bolivia indicates a humidity increase from 2790 cal yr BP, agreeing with our interpretation of Unit-IV. The authors attribute the precipitation increases noted during this period to a southward displacement of the ITCZ (Mayle et al., 2000). Data from the Pumacocha varved lake record between ca. 2150 and 1550 yr BP also support the idea of a SAMS, strengthening the rising humidity verified during this period, as indicated by decreases in the $\delta^{18}\text{O}$ record (Bird et al., 2011), which would have contributed to the increasing humidity seen in Unit-IV.

The high sedimentation event observed in Unit-III, peaking between 1630 and 1460 cal yr BP, is probably related to climatic oscillations with local consequences, such as changes in seasonality. While the general humid trend may be associated to increased precipitation due to a more south-positioned ITCZ, as noted by decreased Ti% in the Cariaco lake record (Haug et al., 2001), and the magnitude of this event may indicate torrential rains. In Northeastern Brazil, the geochemical analysis of Boqueirão Lake indicates a period of high sedimentation rates between 2350 and 1550 cal yr BP, linked to lake margin erosion and high hydrodynamics (Viana et al., 2014), which the authors interpreted as a humid period undergoing an influence from El Niño Southern Oscillation (ENSO) events and variations in the South America Summer Monsoon modulated by the Atlantic SST. ENSO events are less likely to be important in centennial

scales (Novello et al., 2016), so the flood event observed in this unit is probably related to another climatic system. The South American Monsoon System (SAMS) on the other hand, can be affected by insolation in a centennial scale (Novello et al., 2016) and has been shown to be responsible for part of the precipitation pattern in the Amazon region (Garcia and Kayano, 2011; Maksic et al., 2018; Novello et al., 2016). A speleothem recovered from Tamboril cave, in Northeastern Minas Gerais, indicates that the modern $\delta^{18}\text{O}$ value for the SAMS normal behaviour is -5.0 (Wortham et al., 2017). The same study has also indicated that, between 1.678 and 1511 yr BP, the $\delta^{18}\text{O}$ average value was -5.3 , with a minimum value of -6.3 at 1.525 yr BP. The average for this period is slightly below modern average values, which seems to indicate a stronger SAMS activity during this period. As Barro-Preto lake was separated from the river in the previous Unit, the palaeochannel connecting the two dried out, but could still be activated by increased precipitation. As discussed, this inferred connection was not so intense as to alter C:N values or be responsible for an expressive increase in the organic proxies evaluated herein, but was enough to carry coarser sediments to Barro-Preto, as well as charcoal particles, and slightly increase the grain-size of this unit. This modest flood event can, thus, be the result of a small increase in SAMS activity.

A rise in humid conditions in the Amazon during the Late-Holocene has been noted in several studies (e.g. Aniceto et al., 2014; Burbridge et al., 2004; Cordeiro et al., 2008; Mayle et al., 2000). Specifically in Amazon forest-savanna boundaries, Berrio et al. (2000) attested wetter conditions in northwestern Amazon from 875 cal yr BP through pollen analyses. More humid conditions were also detected Saci Lake, located in a rainforest-Cerrado ecotone in southern Amazon, from 1800 to 1300 cal yr BP (Fontes et al., 2017). The Saci lake record is the closest sediment core to Barro-Preto lake, displaying similar $\delta^{13}\text{C}$ values, with an average of -31.8% for this period, which, combined with other proxies, are interpreted as representing the Late-Holocene humid trend. Despite this humidity trend, Saci lake also presents a peak in charcoal particles at around 1300 cal yr BP and a peak in charcoal accumulation rates at ca. 1585 cal yr BP, consistent with charcoal peak values observed in Barro-Preto (Figure 3). The fires suggest the occurrence of eventual dry spells during this period, despite the rising humidity trend.

The palynology of two palm swamp cores in an ecotone in northwestern Amazon indicate that wet conditions prevailed during the recorded period of 1550 cal yr BP (Meneses et al., 2013). Pessenda et al. (1998a, 1998b) demonstrated a forest expansion consistent with a rise in humid conditions during the Late-Holocene, based on carbon isotopes from soil samples. These studies seem to agree that the Late-Holocene presented more humid climatic conditions in the Amazon Basin, including in transitional areas. An expansion of the Amazon biome over the savanna biome is also depicted in an atmospheric general circulation model forced with orbital parameters (Maksic et al., 2018).

Atwood et al. (2014) estimated a southward displacement of the ITCZ between 1400 and 1200 yr BP, which could explain part of the humidity increase in the Amazon in Unit-II, as this region is highly affected by changes in the ITCZ position (Fisch et al., 1996).

Negative SST anomalies in the North Atlantic and Pacific oceans caused by the Atlantic Multidecadal Oscillation (AMO) and the Pacific Decadal Oscillation (PDO, Mann et al., 2009), respectively, could also have contributed to increased moisture availability in the Amazon region in the last 500 years, as observed in Unit-I. The negative phase of AMO is associated with a gradual southward displacement of the ITCZ, while a negative phase of PDO has also been linked to increased precipitation over the Amazon (Limberger et al., 2016). A progressive strengthening of the SAMS throughout the Late-Holocene (Vuille et al., 2012)

could also be responsible for the increased moisture trend found in Barro-Preto lake.

The rising humidity trend observed in BP-1502 may be related, on a larger scale, to an increase in austral summer insolation (Berger and Loutre, 1991). An increase in local insolation may represent higher evapotranspiration and, subsequently, higher moisture recycling for the hydrological cycle (Trenberth et al., 2003) leading to a progressive rise in local precipitation (Salati et al., 1979). Moreover, increased austral summer insolation leads to greater convection and, consequently, higher monsoon and South Atlantic Convergence Zone (SACZ) intensities (Cruz et al., 2005).

While the Amazon Rainforest is associated with high precipitation and general humid conditions, transition regions present in the south and eastern Amazon Rainforest boundaries display a more seasonal climate, characterized by variations in precipitation regimes with dry spells (McMichael et al., 2012a). Dry conditions would favour the spreading of fires ignited by human populations, while more humid periods could hinder the spread of such specific burning. On the other hand, dry conditions would also aid in the spreading of natural lightning-caused fires. In this context, differentiating between anthropogenic induced and natural fires is a complex endeavour. It does, however, seem probable that microcharcoal data from Barro-Preto Lake is associated with dry conditions, typical of transitional environments, whether the origin of the fire is natural or not (e.g. Sifeddine et al., 1994). The microcharcoal data presented a synchronous relationship with charcoal data from other studies performed in the Amazon region (Figure 4).

McMichael et al. (2012a) found signs of anthropic influence in three western Amazon lakes in the Late-Holocene. Combining soil and lake sediment records, that study evidences an increase in agricultural practice and herbaceous species from 3000 cal yr BP, and soil charcoal records fires between 3000 and 1000 cal yr BP at lake Ayauchi (Ecuador). At lakes Gentry and Parker (Peru), peak charcoal deposition occurred between 3700 to 500 cal yr BP at Gentry, in tandem with pollen records of agricultural species, suggesting human influence. At Parker, peak depositions can be observed at ca. 1200 cal yr BP and 500 cal yr BP. Anthropic pressure over the three lake areas diminished since ca. 650 cal yr BP (Gentry), 500 cal yr BP (Ayauchi), and after 250 cal yr BP (Parker), roughly synchronized with the European arrival. This result agrees with the drop in charcoal values seen in the Barro-Preto sequence at ca. 620 cal yr BP. Despite clear human influence concerning forest burning, the authors reported no large-scale land modification by pre-Columbian populations. Another study carried out in lakes Gentry, Parker and Los Amigos revealed more frequent fire return intervals from 2800 to 2600 and 1400 to 1100 cal yr BP. The authors also demonstrated that human impacts on the Amazon Rainforest were intensified by mega Niño droughts that would have increased this area's burning susceptibility, suggesting a combination of human and climatic forces in explaining charcoal records (McMichael et al., 2012b). Soil profiles at Km 41 near Manaus, Central Amazon displayed high charcoal fragment age frequencies, between 1400 and 1200 cal yr BP (Santos et al., 2000).

In the eastern Amazon, two sediment cores retrieved from lakes at the Serra Sul dos Carajás, in the southern portion of the Carajás mountains, indicated the presence of microcharcoal and sponge spicules between 2780 and 1360 cal yr BP, which the authors associated with forest fires due to the occurrence of drier episodes (Sifeddine et al., 1994). In the northern Carajás mountains, Cordeiro et al. (2008) also found evidence of vegetation burning, with an increase in charcoal accumulation rates between 1300 and 70 cal yr BP. Although the probable human presence in the region may have caused forest fires, correlations with the spicules of sponge species adapted to lower lake-levels suggest that

drier conditions were in place. Saci lake, located in the southeastern Amazon region evidenced an increase in black carbon concentration and a reduction in precipitation between 1800 and 1300 cal yr BP, interpreted as a relatively drier period in a still humid climate, with fires probably intensified by a human presence allied to less humid conditions (Fontes et al., 2017, Figure 4).

In the state of Pará, northern Amazon, the geochemical results of lake Comprido indicated maximum charcoal accumulation rate at 1700 cal yr BP, again interpreted as palaeofires from a combined influence of anthropogenic action and drier climate (Cordeiro et al., 2011). In central Guyana, Hammond et al. (2006) detected soil charcoal peaks between 1250 and 1000 yr BP. Despite no archaeological evidence of human settlers, the ages of peak charcoal concentrations are in line with other archaeological studies. The authors argue that drier conditions, possibly linked to a warm El Niño Southern Oscillation phase, would be necessary to spread human-induced fires. Therefore, results reinforce that palaeofires occurred in northern Amazon, especially between 2000 and 1000 yr BP, with unknown intensity but probably caused by an association between human and drier climatic pressures.

At lake Acarabixi, in the northwestern Amazon area, one study reported high charcoal values at ca. 1400 cal yr BP in the sedimentary core. Charcoal records in the Late-Holocene, a much more humid period, alongside pollen evidence of herbs and pioneer species, likely reflects human influence on forest fires. Despite this, the authors also argue that the palaeofires were not enough to alter plant communities in the Late-Holocene (Rodríguez-Zorro et al., 2018).

While high charcoal frequencies are observed mostly in the mid-Holocene in different Amazon regions, especially along the Transamazonian Highway (Soubies, 1980) and in the Upper Rio Negro region, combined with low-lake levels and suggesting dry conditions, remarkably high frequencies of dated charcoals can be seen during the Late-Holocene between 1600 and 1000 cal yr BP, with peak values at 1200 cal yr BP, although alongside relatively higher lake-levels (Hammond et al., 2006; McMichael et al., 2012a; Santos et al., 2000). Some factors can be considered to explain this modern increase in charcoal values, such as greater plant biomass, synergistic action between increased human populations and longer dry seasons or episodic events such as El Niño-like conditions and Atlantic sea surface temperature anomalies, even with annual precipitation rates higher than those in the MH. Additionally, most studies suggest a coupling between human and natural climate influences over palaeofires.

The understanding of lake dynamics associated with the evolution of depositional environments is essential for proxy interpretation (Castro, 2013). In this context, hydrodynamical changes may also be responsible for the general rise-trend in TOC and productivity throughout sediment cores (e.g. Turcq et al., 2002). The Barro-Preto lake formation due to the separation of the meander from its river connection during the Late-Holocene would favour more depositional conditions and increased lake productivity which, in turn, can also be associated to more humid climatic conditions. In this sense, fluvial detachment from the lacustrine sequence is, therefore, critical for a correct palaeoenvironment reconstruction, since variations in the sedimentary constituents associated with changes in sedimentary facies during the river channel migration have no palaeoclimatic meaning. In this study, we consider that the organic constituents of the analysed sediment are representative of lacustrine processes, as no inversions in the core's radiocarbon chronology were observed, which would suggest the input of reworked sediments from several deposits in the basin carried by the Teles Pires river. Furthermore, fluvial C:N ratio values for the Tapajós river, the main river of this basin, were determined as, on average, 6.3 (Kim et al., 2012), much lower than those reported for Barro-Preto in any of the Units (the average value of the entire core is 12.2).

Summary and conclusions

Barro-Preto lake dynamics have changed during the last 3067 cal yr BP. Environmental conditions at Barro-Preto lake were affected by connections with the main stem river, which influenced sedimentation processes and altered the inputs of both clastic and organic material to the lake, not from the river itself but from the neighbouring palaeochannel, activated during intense rain events, characteristic of local sediment processes.

Wet conditions during the Late-Holocene were attested by the analysed organic and sedimentological proxies, consistent with previous studies that indicate a rising humidity trend in the Amazon basin and transitional areas during the Late-Holocene. Within the limitations of bulk OM proxy interpretations, Barro-Preto lake showed no large-scale replacement of Tropical Forest by Cerrado vegetation for the last 3067 cal yr BP, despite being a transitional zone and, hence, more susceptible to changes in Forest-Cerrado boundaries, as noted by the organic proxies. Nevertheless, lake-level changes suggested by this multi-proxy approach are present, related to lake-river dynamics and changes in climate variables. This study highlights the potential of oxbow-lake systems as potential palaeoclimatic change records, as long as the local hydrodynamic and sedimentation processes are well understood and accounted for.

Despite the increasing humidity trend observed for the Late-Holocene, episodic dry events may have occurred, as suggested by Barro-Preto lake microcharcoal data, agreeing with previous studies for the Amazon (Cordeiro et al., 2011; Fontes et al., 2017; Hammond et al., 2006; McMichael et al., 2012a, 2012b; Rodríguez-Zorro et al., 2018; Santos et al., 2000). These dry events may be related to El Niño-like conditions and Atlantic SST anomalies, as it is well known that variations in these modes affect the Amazon climate (e.g. Fisch et al., 1996; Jimenez et al., 2019; Limberger and Silva, 2016; Marengo et al., 2013; Silva et al., 2009). More research is required to adequately estimate human impacts on transitional zones between the Amazon Rainforest and Cerrado biome, determine specific lake-level variations and better understand species-level responses of this ecotone to climate change. We especially recommend research interconnecting forest fire evidence, archaeological sites and compositional vegetation changes.

Acknowledgements

The authors would like to thank the French Research Institute for Development (IRD) for supporting radiocarbon dating costs. We also thank two anonymous reviewers who greatly contributed to the improvement of the submitted manuscript.

Funding

The author(s) disclosed receipt of the following financial support for the research, authorship, and/or publication of this article: This study was financed in part by the Coordenação de Aperfeiçoamento de Pessoal de Nível Superior – Brasil (CAPES) – Finance Code 001, CLIMATE-PRINTUFF Project – Grant 88887.310301/2018-00 and also supported by CNPq (Conselho Nacional de Desenvolvimento Científico e Tecnológico from Brazil), processes 134803/2016-7, 423573/2018-7, 308769/2018-0 and by FAPERJ (Fundação Carlos Chagas Filho de Amparo à Pesquisa do Estado do Rio de Janeiro), process 201.916/2017.

ORCID iD

Kury Milena Souza  <https://orcid.org/0000-0003-0501-9440>

References

- Absy ML, Cleef AM, Fournier M et al. (1991) Mise en évidence de quatre phases d'ouverture de la forêt dense dans le sud-est de l'Amazonie au cours des 60000 dernières années. Première comparaison avec d'autres régions tropicales. *C. R. Académie des Sciences Paris* 312(2): 673–678.

- Alencar A, Nepstad DC and Del Carmen Vera Diaz M (2006) Forest understory fire in the Brazilian Amazon in ENSO and non-ENSO years: Area burned and committed carbon emissions. *Earth Interactions* 10: 6.
- Aniceto K, Moreira-Turcq P, Cordeiro RC et al. (2014) Hydrological changes in West Amazonia over the Past 6 Ka inferred from geochemical proxies in the sediment record of a floodplain lake. *Procedia Earth and Planetary Science* 10: 287–291.
- Araújo RDEA (2008) *Florística e estrutura em fragmento florestal urbano no município de Sinop, Mato Grosso*. Master Thesis, Universidade Federal do Mato Grosso, BR.
- Araújo-Lima CA, Forsberg BR, Victoria R et al. (1986) Energy sources for detritivorous fishes in the Amazon. *Science* 234(4781): 1256–1258.
- Atwood AR and Sachs JP (2014) Separating ITCZ- and ENSO-related rainfall changes in the Galápagos over the last 3 kyr using D/H ratios of multiple lipid biomarkers. *Earth and Planetary Science Letters* 404: 408–419.
- Behling H and Hooghiemstra H (2000a) Holocene Amazon rainforest – Savanna dynamics and climatic implications: High-resolution pollen record from Laguna Loma Linda in eastern Colombia. *Journal of Quaternary Science* 15(7): 687–695.
- Behling H and Hooghiemstra H (2000b) Neotropical savanna environments in space and time: Late quaternary interhemispheric comparisons. In: *Interhemispheric Climate Linkages*. New York, NY: Academic Press, pp.307–323.
- Berger A and Loutre MF (1991) Insolation values for the climate of the last 10 million years. *Quaternary Science Reviews* 10(4): 297–317.
- Berrio JC, Hooghiemstra H, Behling H et al. (2000) Late-Holocene history of savanna gallery forest from Carimagua area, Colombia. *Review of Palaeobotany and Palynology* 111: 295–308.
- Bird BW, Abbott MB, Vuille M et al. (2011) A 2,300-year-long annually resolved record of the South American summer monsoon from the Peruvian Andes. *Proceedings of the National Academy of Sciences* 108(21): 8583–8588.
- Blaauw M (2010) Methods and code for ‘classical’ age-modelling of radiocarbon sequences. *Quaternary Geochronology* 5: 512–518.
- Burbridge RE, Mayle FE and Killeen TJ (2004) Fifty-thousand-year vegetation and climate history of Noel Kempff Mercado National Park, Bolivian Amazon. *Quaternary Research* 61(2): 215–230.
- Bush MB and de Oliveira PE (2006) The rise and fall of the Refugial Hypothesis of Amazonian speciation: A paleoecological perspective. *Biota Neotropica* 6: 1.
- Bush MB, De Oliveira PE, Colinvaux PA et al. (2004) Amazonian paleoecological histories: one hill, three watersheds. *Palaeogeography, Palaeoclimatology, Palaeoecology* 214: 359–393.
- Bush MB, Silman MR, de Toledo MB et al. (2007) Holocene fire and occupation in Amazonia: Records from two lake districts. *Philosophical Transactions of the Royal Society B: Biological Sciences* 362(1478): 209–218.
- Castro DF, de Oliveira PE, Rossetti DF et al. (2013) Late Quaternary landscape evolution of northeastern Amazonia from pollen and diatom records. *Anais da Academia Brasileira de Ciências* 85(1): 35–55.
- Cheng H, Sinha A, Cruz FW et al. (2013) Climate change patterns in Amazonia and biodiversity. *Nature Communications* 4: 1411.
- Colinvaux PA, De Oliveira PE, Moreno JE et al. (1996) A long pollen record from lowland Amazonia: Forest and cooling in glacial times. *Science, New Series* 274(October): 85–88.
- Cordeiro RC, Turcq B, Sifeddine A et al. (2011) Biogeochemical indicators of environmental changes from 50Ka to 10Ka in a humid region of the Brazilian Amazon. *Palaeogeography, Palaeoclimatology, Palaeoecology* 299(3–4): 426–436.
- Cordeiro RC, Turcq B, Suguio K et al. (2008) Holocene fires in East Amazonia (Carajás), new evidences, chronology and relation with paleoclimate. *Global and Planetary Change* 61(1–2): 49–62.
- Cordeiro RC, Turcq B, Suguio K et al. (1997) Holocene environmental changes in Carajás Region (Pará, Brazil) recorded by lacustrine deposits. *SIL Proceedings 1922–2010* 26(2): 814–817.
- Cruz FW, Burns SJ, Karmann I et al. (2005) Insolation-driven changes in atmospheric circulation over the past 116,000 years in subtropical Brazil. *Nature* 434(7029): 63–66.
- De Toledo MB and Bush MB (2008) Vegetation and hydrology changes in Eastern Amazonia inferred from a pollen record. *Anais da Academia Brasileira de Ciências* 80(1): 191–203.
- Desjardins T (1996) Changes of the forest-savanna boundary in Brazilian Amazonia during. *The Holocene* 108: 749–756.
- Esteves FDA (1998) *Fundamentos de Limnologia*, 2nd edn. Rio de Janeiro, Brazil: Interciência Finep.
- Fisch G, Marengo JA and Nobre CA (1996) Clima da amazônia. *Climanálise* 10: 24–41.
- Fogel ML and Cifuentes LA (1993) Isotope fractionation during primary production. In: Engel MH and Macko SA (eds). *Organic Geochemistry*. New York: Plenum Press, pp.73–98.
- Fontes D, Cordeiro RC, Martins GS et al. (2017) Paleoenvironmental dynamics in South Amazonia, Brazil, during the last 35,000 years inferred from pollen and geochemical records of Lago do Saci. *Quaternary Science Reviews* 173: 161–180.
- Garcia SR and Kayano MT (2011) Moisture and heat budgets associated with the South American monsoon system and the Atlantic ITCZ. *International Journal of Climatology* 31: 2154–2167.
- Hammer Ø, Harper DAT and Ryan PD (2001) PAST: Paleontological statistics software package for education and data analysis. *Paleontologia Eletrônica* 4(1): 1–9.
- Hammond DS, Ter Steege H and Van Der Borg K (2006) Upland soil charcoal in the wet tropical forests of central Guyana. *Biotropica* 39(2): 153–160.
- Haug GH, Hughen KA, Sigman DM et al. (2001) Southward migration of the intertropical convergence zone through the Holocene. *Science* 293(August): 1304–1308.
- Hogg AG, Heaton TJ, Hua Q et al. (2020) SHCal20 southern hemisphere calibration, 0–55,000 years cal BP. *Radiocarbon* 62: 759–778.
- Hudson PF, Heitmuller FT and Leitch MB (2012) Hydrologic connectivity of oxbow lakes along the lower Guadalupe River, Texas: The influence of geomorphic and climatic controls on the ‘flood pulse concept’. *Journal of Hydrology* 414–415: 174–183.
- Instituto Nacional de Meteorologia (INMET) (2019) Estação Meteorológica de Observação de Superfície Convencional. Available at: <http://www.inmet.gov.br/portal/index.php?r=estacoes/estacoesConvencionais/> (accessed on February 2019).
- Jimenez JC, Marengo JA, Alves LM et al. (2019) The role of ENSO flavours and TNA on recent droughts over Amazon forests and the Northeast Brazil region. *International Journal of Climatology*. Epub ahead of print 17 December 2019. DOI: 10.1002/joc.6453.
- Kim JH, Zella C, Moreira-Turcq P et al. (2012) Tracing soil organic carbon in the lower Amazon River and its tributaries using GDGT distributions and bulk organic matter properties. *Geochimica et Cosmochimica Acta* 90: 163–180.
- Limberger L and Silva MES (2016) Precipitação na bacia amazônica e sua associação à variabilidade da temperatura

- da superfície dos oceanos Pacífico e Atlântico: uma revisão. *GEOUSP: Espaço e Tempo (Online)* 20(3): 657–675.
- Maezumi SY, Alves D, Robinson M et al. (2018) The legacy of 4,500 years of polyculture agroforestry in the eastern Amazon. *Nature Plants* 4(8): 540–547.
- Maksic J, Shimizu MH, de Oliveira GS et al. (2018) Simulation of the Holocene climate over South America and impacts on the vegetation. *The Holocene* 29(2): 1–13.
- Mann ME, Zhang Z, Rutherford S et al. (2009) Global signatures and dynamical origins of the little ice age and medieval climate anomaly. *Science* 326(5957): 1256–1260.
- Marengo JA, Alves LM, Soares WR et al. (2013) Two contrasting severe seasonal extremes in tropical South America in 2012: Flood in Amazonia and drought in Northeast Brazil. *Journal of Climate* 26(22): 9137–9154.
- Mayle FE, Burbridge RE and Killeen TJ (2000) Millennial-scale dynamics of southern Amazonian rain forests. *Science, New Series* 290(5500): 2291–2294.
- McMichael CH, Bush MB, Piperno DR et al. (2012a) Spatial and temporal scales of pre-Columbian disturbance associated with western Amazonian lakes. *Holocene* 22(2): 131–141.
- McMichael CH, Correa-Metrio A and Bush MB (2012b) Pre-Columbian fire regimes in lowland tropical rainforests of southeastern Peru. *Palaeogeography, Palaeoclimatology, Palaeoecology* 342–343: 73–83.
- Meneses ME, Lima da Costa M and Behling H (2013) Journal of South American Earth Sciences Late-Holocene vegetation and fire dynamics from a savanna-forest ecotone in Roraima state, northern Brazilian Amazon. *Journal of South American Earth Sciences* 42: 17–26.
- Meyers P (2003) Application of organic geochemistry to paleolimnological reconstruction: A summary of examples from the Laurentian Great Lakes. *Organic Geochemistry* 34: 261–289.
- Meyers PA and Eadie BJ (1993) Sources, degradation and recycling of organic matter associated with sinking particles in Lake Michigan. *Organic Geochemistry* 20(1): 47–56.
- Meyers PA and Lallier-Vergès E (1999) Lacustrine sedimentary organic matter records of late quaternary paleoclimates. *Journal of Paleolimnology* 21: 345–372.
- Meyers PA and Teranes JL (2001) Sediment organic matter. *Tracking Environmental Change Using Lake Sediments* 2(1999): 239–269.
- Moreira LS, Moreira-Turcq P, Cordeiro RC et al. (2013a) Holocene paleoenvironmental reconstruction in the Eastern Amazonian Basin: Comprido Lake. *Journal of South American Earth Sciences* 44: 55–62.
- Moreira LS, Moreira-Turcq P, Turcq B et al. (2013b) Palaeohydrological controls on sedimentary organic matter in an Amazon floodplain lake, Lake Maraca (Brazil) during the Late-Holocene. *The Holocene* 23(12): 1903–1914.
- Moreira-Turcq P, Turcq B, Moreira LS et al. (2014) A 2700 cal yr BP extreme flood event revealed by sediment accumulation in Amazon floodplains. *Palaeogeography, Palaeoclimatology, Palaeoecology* 415: 175–182.
- Munsell AH (2000). *Munsell Soil Color Charts*. New Windsor, NY: Munsell Color.
- Nevle RJ and Bird DK (2008) Effects of syn-pandemic fire reduction and reforestation in the tropical Americas on atmospheric CO₂ during European conquest. *Palaeogeography, Palaeoclimatology, Palaeoecology* 264: 25–38.
- Nolan C, Allen JRM and Anderson P (2018) Past and future global transformation of terrestrial ecosystems under climate change. *Science* 361: 920–923.
- Novello VF, Vuille M, Cruz FW et al. (2016) Centennial-scale solar forcing of the South American Monsoon System recorded in stalagmites. *Scientific Reports* 6(1): 24762.
- Olivares I, Svenning J, Van Bodegom PM et al. (2015) Effects of warming and drought on the vegetation and plant diversity in the amazon basin. *Biological Reviews* 81: 42–69.
- Pessenda LCR, Boulet R, Aravena R et al. (2001) Origin and dynamics of soil organic matter and vegetation changes during the Holocene in a forest-savanna transition zone, Brazilian Amazon region. *The Holocene* 11(2): 250–254.
- Pessenda LCR, Gomes BM, Aravena R et al. (1998b) The carbon isotope record in soils along a forest-cerrado ecosystem transect: implication for vegetation changes in Rondônia State, southwestern Brazilian Amazon region. *The Holocene* 8(May): 631–635.
- Pessenda LCR, Gouveia SEM, Aravena R et al. (1998a) 14C dating and stable carbon isotopes of soil organic matter in forest-savanna boundary areas in the southern Brazilian. *Radiocarbon* 40(2): 1013–1022.
- Rein B, Lückge A and Sirocko F (2004) A significant Holocene ENSO anomaly during the Medieval period. *Geophysical Research Letters* 31(17): 2–5.
- Reuter J, Stott L, Khider D et al. (2009) A new perspective on the hydroclimate variability in northern South America during the Little Ice Age. *Geophysical Research Letters* 36(21): 1–5.
- Richards P (2018) It's not just where you farm; It's whether your neighbor does too. How agglomeration economies are shaping new agricultural landscapes. *Journal of Economic Geography* 18(1): 87–110.
- Rodriguez-Zorro PA, Turcq B, Cordeiro RC et al. (2018) Forest stability during the early and Late-Holocene in the igapó floodplains of the Rio Negro, northwestern Brazil. *Quaternary Research (United States)* 89(1): 75–89.
- Salati E, Dall'Olio A, Matsu E et al. (1979) Recycling of water in the Amazon Basin: An isotopic study. *Water Resources Research* 15(5): 1250–1258.
- Santos GM, Rom W, Golser R et al. (2000) 14C AMS dating of fires in the central Amazon rain forest. *Nuclear Instruments and Methods in Physics Research Section B: Beam Interactions with Materials and Atoms* 172: 761–766.
- Sifeddine A, Bertrand P, Fournier M et al. (1994) La sédimentation organique lacustre en milieu tropical humide (Carajas, Amazonie orientale, Brésil): relation avec les changements climatiques au cours des 60000 dernières années. *Bulletin de la Société Géologique de France* 165(6): 613–621.
- Silva GAM, Ambrizzi T and Marengo JA (2009) Observational evidences on the modulation of the South American low level jet east of the Andes according the ENSO variability. *Annales Geophysicae* 27(2): 645–657.
- Silverio DV, Brando PM, Balch JK et al. (2013) Testing the Amazon savannization hypothesis: fire effects on invasion of a neotropical forest by native cerrado and exotic pasture grasses. *Philosophical Transactions of the Royal Society B: Biological Sciences* 368(1619): 20120427. DOI: 10.1098/rstb.2012.0427.
- Simoes R, Picoli MCA, Camara G et al. (2020) Land use and cover maps for Mato Grosso State in Brazil from 2001 to 2017. *Scientific Data* 7(1): 1–10.
- Soubies F (1980) Existence of a dry phase in the Brazilian Amazon by the presence of charcoal (6000–3000 years B.P.). *Cahiers ORSTOM, Serie Géologie* 11(1): 133–148.
- Staver AC, Archibald S and Levin SA (2011) The global extent and determinants of savanna and forest as alternative biome states. *Science* 334(6053): 230–232.
- Trenberth KE, Dai A, Rasmussen RM et al. (2003) The changing character of precipitation. *American Meteorological Society* 83(9): 1205–1218.
- Turcq B, Albuquerque ALS, Cordeiro RC et al. (2002) Accumulation of organic carbon in five Brazilian lakes during the Holocene. *Sedimentary Geology* 148(1–2): 319–342.

- Udden JA (1914) Mechanical composition of clastic sediments. *Bulletin of the Geological Society of America* 25: 655–744.
- Vallentyne JR (1955) Sedimentary chlorophyll determination as a paleobotanical method. *Canadian Journal of Botany* 33(4): 304–313.
- Van Der Hammen T and Hooghiemstra H (2000) Neogene and quaternary history of vegetation, climate, and plant diversity in Amazonia. *Quaternary Science Reviews* 19(8): 725–742.
- Van Rossum G and Drake FL (2009) *Python 3 Reference Manual*. Scotts Valley, CA: CreateSpace.
- Viana JCC, Sifeddine A, Turcq B et al. (2014) A late-Holocene paleoclimate reconstruction from Boqueirão Lake sediments, northeastern Brazil. *Palaeogeography, Palaeoclimatology, Palaeoecology* 415: 117–126.
- Vidotto E, Carlos L, Pessenda LCR et al. (2007) Dinâmica do ecótono floresta-campo no sul do estado do Amazonas no Holoceno, através de estudos isotópicos e fitossociológicos. *Acta Amazonica* 37(3): 385–400.
- Vuille M, Burns SJ, Taylor BL et al. (2012) A review of the South American monsoon history as recorded in stable isotopic proxies over the past two millennia. *Climate of the Past* 8(4): 1309–1321.
- Wentworth CK (1922) A scale of grade and class terms for clastic sediments. *Journal of Geology* 30: 377–392.
- Wolff EW, Chappellaz J, Blunier T et al. (2010) Millennial-scale variability during the last glacial: The ice core record. *Quaternary Science Reviews* 29(21–22): 2828–2838.
- Worham BE, Wong CI, Silva LCR et al. (2017) Assessing response of local moisture conditions in central Brazil to variability in regional monsoon intensity using speleothem $^{87}\text{Sr}/^{86}\text{Sr}$ values. *Earth and Planetary Science Letters* 463: 310–322.
- Wren DG, Davidson GR, Walker WG et al. (2014) The evolution of an oxbow lake in the Mississippi alluvial floodplain. *Journal of Soil and Water Conservation* 63(3): 129–135.